Hindawi
Mathematical Problems in Engineering
Volume 2018, Article ID 6538610, 13 pages
https://doi.org/10.1155/2018/6538610

Research Article

Image Restoration by a Mixed High-Order Total Variation and l_1 Regularization Model

Jianguang Zhu,[1] **Kai Li**,[1] **and Binbin Hao**[2]

[1]*College of Mathematics and Systems Science, Shandong University of Science and Technology, Qingdao 266590, China*
[2]*College of Science, China University of Petroleum, Qingdao 266580, China*

Correspondence should be addressed to Binbin Hao; bbhao981@163.com

Received 14 June 2018; Revised 16 August 2018; Accepted 29 August 2018; Published 24 September 2018

Academic Editor: Chris Goodrich

Total variation regularization is well-known for recovering sharp edges; however, it usually produces staircase artifacts. In this paper, in order to overcome the shortcoming of total variation regularization, we propose a new variational model combining high-order total variation regularization and l_1 regularization. The new model has separable structure which enables us to solve the involved subproblems more efficiently. We propose a fast alternating method by employing the fast iterative shrinkage-thresholding algorithm (FISTA) and the alternating direction method of multipliers (ADMM). Compared with some current state-of-the-art methods, numerical experiments show that our proposed model can significantly improve the quality of restored images and obtain higher SNR and SSIM values.

1. Introduction

Image restoration is an important and fundamental problem in the literature of image processing. It is widely used in many fields, such as machine identification, biomedicine, astronomy, and medical imaging [1–4]. The purpose of image restoration is to get a better visual image from the degraded image. There are many factors that cause image degradation, for instance, atmospheric turbulence, camera shake, and the relative motion between an imaging device and an object [5].

The typical representation of image degradation is the blurring and additional noise of image. The original model of image degradation can generally be defined as

$$g = Ku + \eta, \tag{1}$$

where u is an original image, K is a blur operator, η is an additive noise, and g is a degraded image. Our aim is to recover u from g, which is known as deconvolution or deblurring.

Recovering u from g is a typically ill-posed problem. So we cannot solve it simply by using the normal least-squares method. In order to overcome the ill-condition of the problem, adding some regularization terms to the energy functional is usually adopted. One of the commendable regularization methods is Tikhonov regularization [6]. However, this method often tends to make images overly smooth and fails to preserve image details. In order to overcome this shortcoming, in 1992, replacing L_2-norm of u with the TV-norm of u, Rudin, Osher, and Fatemi in [7] introduced the following famous Rudin-Osher-Fatemi (ROF) model:

$$\min_u \|Ku - g\|_2^2 + \alpha \|u\|_{TV}, \tag{2}$$

where $\|\cdot\|_2$ denotes the Euclidean norm, the first term of (2) is called fidelity term, and $\|\cdot\|_{TV}$ is the total variation regularization term. α is a positive regularization parameter which controls the trade-off between the first and second terms. The isotropic discrete total variation regularization term can be defined as

$$\|u\|_{TV} = \sum_{1\le i,j\le n} \sqrt{\left|(\nabla u)_{i,j}^x\right|^2 + \left|(\nabla u)_{i,j}^y\right|^2}, \tag{3}$$

where ∇ denotes the discrete gradient operator which is defined as follows:

$$(\nabla u)_{i,j} = \left((\nabla u)_{i,j}^x, (\nabla u)_{i,j}^y\right), \tag{4}$$

with

$$(\nabla u)^x_{i,j} = \begin{cases} u_{i+1,j} - u_{i,j} & if\ i < n, \\ u_{1,j} - u_{n,j} & if\ i = n, \end{cases}$$
$$(\nabla u)^y_{i,j} = \begin{cases} u_{i,j+1} - u_{i,j} & if\ j < n, \\ u_{i,1} - u_{i,n} & if\ j = n, \end{cases} \quad (5)$$

for $i, j = 1, \ldots, n$. Here $u_{i,j}$ refers to the $((j-1)n + i)th$ entry of the vector u. It is the $(i, j)th$ pixel location of the image; see [8].

As well known, TV function is nondifferentiable and nonlinear; it is difficult to solve the ROF model (2). A number of efficient and robust methods are proposed to solve the ROF model. In [7], by seeking the steady-state solution of a parabolic PDE, Rudin et al. proposed a time marching scheme to solve the associated Euler-Lagrange equation of (2). In [8, 9], a lagged diffusivity fixed point iteration method was proposed to solving the same problem. Later, Newton's method [10–15] and Chambolle's projection algorithm [16–18] were proposed. Another class of algorithms for TV problems are the iterative shrinkage/thresholding (IST) algorithms, which are independently proposed and analyzed by several authors in different fields [19–24]. Recently, some first-order optimization methods were proposed, such as fast TV deconvolution algorithm (FTVd) [25], augmented Lagrangian method (ALM), and split Bregman method [26–29]. Alternating direction method (ADM) [30–32], which is a variant of the ALM, goes back to the work of Gabay and Mercier [33]. The ADM was first studied extensively in variational optimization problems and then introduced to the fields of image processing [30, 31]. There are also many other methods for image restoration, such as partial differential equation (PDE) based methods [34–40] and the neural network methods [41, 42].

Recently, to further study the solving methods for ROF model, Huang et al. [46] introduced a new auxiliary variable f and proposed a fast total variation minimization method as follows:

$$\min_{u,f} \|Ku - g\|_2^2 + \alpha_1 \|u - f\|_2^2 + \alpha_2 \|f\|_{TV}, \quad (6)$$

where α_1, α_2 are positive regularization parameters. The main purpose of this model (6) is to realize the separation of denoising and deblurring steps. The authors solved system (6) by an alternating minimization algorithm. The experimental results show the effectiveness of their method. In the process of image processing, there are some abnormal values, such as the sudden jump of pixels in a certain area. However, l_1 regularization is less sensitive to abnormal values and promotes sparse solutions. In [44], an unconstrained l_1 regularized minimization problem was proposed:

$$\min_{u,f} \|Ku - g\|_2^2 + \alpha_1 \|u - f\|_2^2 + \alpha_2 \|u\|_1 + \alpha_3 \|f\|_{TV}, \quad (7)$$

where $\alpha_1, \alpha_2, \alpha_3$ are positive regularization parameters. Due to l_1 and TV norm used in model (7), the experimental results show a good recovery effect.

It has been shown in [47, 48] that total variation methods can realize significantly sharper edges and overall more visually pleasing images. However, on the other hand, they tend to create piecewise-constant images even in regions with smooth transitions of grey or color values in the original image. The undesired artifact is usually called staircase effect. Staircase solution fails to satisfy the evaluation of visual quality and develops false edges that do not exist in the true image.

To overcome the adverse effects in the application of image processing, a popular method is to replace the TV norm by a higher-order TV norm [45, 49–52]. Lysaker et al. first proposed second-order total variation regularizer in [53] for additive noise removal in the process of medical image processing. Their method shows robustness in the protection of the edges. Later, a second-order model to substantially reduce the staircase effect was proposed by Chan et al. in [48]. In particular, the second-order TV regularization schemes are widely studied to overcome the staircase effects while preserving the edges well in the restored image.

Recently, Lv et al. in [45] proposed a high-order total variation minimization model:

$$\min_{u,f} \|Ku - g\|_2^2 + \alpha_1 \|u - f\|_2^2 + \alpha_2 \|f\|_{HTV}, \quad (8)$$

where α_1, α_2 are positive regularization parameters and $\|f\|_{HTV}$ denotes higher-order total variation. The minimization model can reduce the staircase effect in the process of image restoration. The authors adopted an alternating minimization algorithm to solve the high-order minimization problem (8). Their experimental results showed that the proposed method gave the restored images with higher quality than some existing first-order total variation restoration methods.

Motivated by the works of [44–46], we propose a new unconstrained minimization model:

$$\min_{u,f} \|Ku - g\|_2^2 + \alpha_1 \|u - f\|_2^2 + \alpha_2 \|u\|_1 + \alpha_3 \|f\|_{HTV}, \quad (9)$$

where α_1, α_2, and α_3 are positive regularization parameters. The definition of second-order total variation is similar to the definition of the first-order one:

$$\left(\nabla^2 f\right)_{i,j} = \left((\nabla f)^{x,x}_{i,j}, (\nabla f)^{x,y}_{i,j}, (\nabla f)^{y,x}_{i,j}, (\nabla f)^{y,y}_{i,j}\right),$$
$$\left\|\nabla^2 f\right\| = \sum_{1 \le i,j \le n} \sqrt{\left|(\nabla f)^{x,x}_{i,j}\right|^2 + \left|(\nabla f)^{x,y}_{i,j}\right|^2 + \left|(\nabla f)^{y,x}_{i,j}\right|^2 + \left|(\nabla f)^{y,y}_{i,j}\right|^2}, \quad (10)$$

where $(\nabla f)^{x,x}_{i,j}, (\nabla f)^{x,y}_{i,j}, (\nabla f)^{y,x}_{i,j}, (\nabla f)^{y,y}_{i,j}$ denote the second-order discrete gradient of the $((j-1)n + i)th$ entry of the vector f. For more details about the second-order difference, refer to [54]. The second-order TV regularization and l_1 regularization are used; the edges in the restored image can be preserved quite well and the staircase effect is reduced simultaneously. An alternating minimization method is used to solve the new unconstrained minimization model (9). By comparing with the other existing methods about total

variation, our numerical experiments show the effectiveness of the minimization model (9).

The rest of this paper is organized as follows. In Section 2, we propose our alternating minimization algorithm to solve model (9), which is based on the fast iterative shrinkage-thresholding algorithm (FISTA) and the alternating direction method of multipliers (ADMM). In Section 3, we give some numerical results to demonstrate the effectiveness of the proposed algorithm. Finally, concluding remarks of this paper are given in Section 4.

2. Alternating Minimization Method

In this section, we apply the ADMM idea to derive an algorithm for solving problem (9). We first introduce an auxiliary variable ω to transform problem (9) into an equivalent constrained optimization problem,

$$\begin{aligned} \min_{u,f,\omega} \quad & \|Ku-g\|_2^2+\alpha_1\|u-f\|_2^2+\alpha_2\|u\|_1+\alpha_3\|\omega\|_2, \\ \text{s.t.} \quad & \omega=\nabla^2 f, \end{aligned} \tag{11}$$

and then minimize the augmented Lagrangian function of problem (11) by using the fast iterative shrinkage-thresholding algorithm and the alternating direction multiplier method.

For the above constrained optimization problem (11), its augmented Lagrange function is defined by

$$\begin{aligned} L_A(u,f,\omega,\gamma)=\min_{u,f}\ & \|Ku-g\|_2^2+\alpha_1\|u-f\|_2^2 \\ & +\alpha_2\|u\|_1+\alpha_3\|\omega\|_2-\gamma^T\left(\omega-\nabla^2 f\right) \\ & +\frac{\beta}{2}\left\|\omega-\nabla^2 f\right\|_2^2. \end{aligned} \tag{12}$$

Then, using the alternating minimization method to solve problem (12) can be expressed as follows:

$$\begin{aligned} u^{k+1}&=\arg\min_u L_A\left(u,f^k,\omega^k,\gamma^k\right) \\ \omega^{k+1}&=\arg\min_\omega L_A\left(u^{k+1},f^k,\omega,\gamma^k\right) \\ f^{k+1}&=\arg\min_f L_A\left(u^{k+1},f,\omega^{k+1},\gamma^k\right) \\ \gamma^{k+1}&=\gamma^k-\beta\left(\omega^{k+1}-\nabla^2 f^{k+1}\right). \end{aligned} \tag{13}$$

Fixing f^k, ω^k, the u subproblem can be obtained by solving the following minimization problem. Recently, various acceleration techniques of iterative algorithms are proposed [55–63]. For this subproblem, in order to accelerate the convergence of the above iteration, we adopt the acceleration technique in [55] to solve it.

$$\begin{aligned} u^{k+1}&=\arg\min_u \|Ku-g\|_2^2+\alpha_1\left\|u-f^k\right\|_2^2+\alpha_2\|u\|_1 \\ &=\arg\min_u\left\{\alpha_2\|u\|_1+\frac{L}{2}\|u-z\|^2\right\}, \end{aligned} \tag{14}$$

where

$$\begin{aligned} z&=y^{k+1}-\frac{2}{L}\left(K^TKy^{k+1}-K^Tg+\alpha_1\left(y^{k+1}-f^k\right)\right), \\ y^{k+1}&=u^k+\left(\frac{t^k-1}{t^{k+1}}\right)\left(u^k-u^{k-1}\right), \\ t^{k+1}&=\frac{1+\sqrt{1+4\left(t^k\right)^2}}{2}, \end{aligned} \tag{15}$$

L is a Lipschitz constant [55], and $t^0=1$. So, the minimizer of u is given by the one-dimensional shrinkage:

$$u^{k+1}=\max\left(|z|-\frac{\alpha_2}{L},0\right)\operatorname{sgn}(z). \tag{16}$$

Fixing f^k, u^{k+1}, the subproblem for ω is equivalent to

$$\begin{aligned} \omega^{k+1}&=\arg\min_\omega \alpha_3\|\omega\|_2-\left(\gamma^k\right)^T\left(\omega-\nabla^2 f^k\right) \\ &\quad+\frac{\beta}{2}\left\|\omega-\nabla^2 f^k\right\|_2^2 \\ &=\arg\min_\omega \frac{\beta}{2}\left\|\omega-\left(\nabla^2 f^k+\frac{\gamma^k}{\beta}\right)\right\|_2^2+\alpha_3\|\omega\|_2. \end{aligned} \tag{17}$$

According to [64], the solution of ω can be obtained by the two-dimensional shrinkage:

$$\omega^{k+1}=\max\left\{\left\|\nabla^2 f^k+\frac{\gamma^k}{\beta}\right\|-\frac{\alpha_3}{\beta},0\right\}\frac{\nabla^2 f^k+\gamma^k/\beta}{\left\|\nabla^2 f^k+\gamma^k/\beta\right\|}, \tag{18}$$

where the convention $0\cdot(0/0)=0$ is followed.

Fixing u^{k+1}, ω^{k+1}, the subproblem for f can be written as follows:

$$\begin{aligned} f^{k+1}&=\arg\min_f \alpha_1\left\|u^{k+1}-f\right\|_2^2-\left(\gamma^k\right)^T\left(\omega^{k+1}-\nabla^2 f\right) \\ &\quad+\frac{\beta}{2}\left\|\omega^{k+1}-\nabla^2 f\right\|_2^2 \\ &=\arg\min_f \alpha_1\left\|u^{k+1}-f\right\|_2^2 \\ &\quad+\frac{\beta}{2}\left\|\omega^{k+1}-\left(\nabla^2 f^k+\frac{\gamma^k}{\beta}\right)\right\|_2^2. \end{aligned} \tag{19}$$

We can get the exact minimizer solution from the optimal conditions of (19) as follows:

$$\begin{aligned} &\left(2\alpha_1 I+\beta\nabla^{2^T}\nabla^2\right)f^{k+1} \\ &\quad=2\alpha_1 u^{k+1}+\beta\nabla^{2^T}\omega^{k+1}-\nabla^{2^T}\gamma^k, \end{aligned} \tag{20}$$

where ∇ refers to the first-order difference operator and ∇^{2^T} is the adjoint of ∇^2. I represents the identity matrix.

(1) Input: $g, K, \alpha_1 > 0, \alpha_2 > 0, \alpha_3 > 0, \beta > 0$ and γ^0
(2) Initialization: $f^0 = g, u^0 = g, \omega^0 = \nabla^2 f^0$
(3) **While** $\|f^{k+1} - f^k\|_2^2 / \|f^k\|_2^2 > \varepsilon$ and $k < Maxiter$, **Do**
(4) Compute u^{k+1} from (14).

$$u^{k+1} = \max\left(|z| - \frac{\alpha_2}{L}, 0\right) sgn(z),$$

(5) Compute ω^{k+1} from (17).

$$\omega^{k+1} = \max\left\{\left\|\nabla^2 f^k + \frac{\gamma^k}{\beta}\right\| - \frac{\alpha_1}{\beta}, 0\right\} \frac{\nabla^2 f^k + \gamma^k/\beta}{\left\|\nabla^2 f^k + \gamma^k/\beta\right\|},$$

(6) Compute f^{k+1} via solving (20).

$$f^{k+1} = \mathcal{F}^{-1}\left\{\frac{2\alpha_1 \mathcal{F}\left(u^{k+1}\right) + \beta\mathcal{F}\left(\nabla_x^2\right)^* \circ \mathcal{F}\left(\omega_x^{k+1}\right) + \beta\mathcal{F}\left(\nabla_y^2\right)^* \circ \mathcal{F}\left(\omega_y^{k+1}\right) - \mathcal{F}\left(\nabla_x^2\right)\gamma_1^k - \mathcal{F}\left(\nabla_y^2\right)\gamma_2^k}{2\alpha_1 \mathcal{F}(I) + \beta\mathcal{F}\left(\nabla_x^2\right)^* \circ \mathcal{F}\left(\nabla_x^2\right) + \beta\mathcal{F}\left(\nabla_y^2\right)^* \circ \mathcal{F}\left(\nabla_y^2\right)}\right\},$$

(7) Update γ^{k+1} from (22).

$$\gamma^{k+1} = \gamma^k - \beta(\omega^{k+1} - \nabla^2 f^{k+1}).$$

(8) **End Do**

Algorithm 1

Assuming that the problem satisfies the periodic boundary condition, then $\nabla^{2^T}\nabla^2$ is block circulant matrix [65, 66], which can be diagonalized by the two-dimensional discrete Fourier transform. So, by using the convolution theorem, we get

$$f^{k+1} = \mathcal{F}^{-1}\left\{\frac{2\alpha_1 \mathcal{F}\left(u^{k+1}\right) + \beta\mathcal{F}\left(\nabla_x^2\right)^* \circ \mathcal{F}\left(\omega_x^{k+1}\right) + \beta\mathcal{F}\left(\nabla_y^2\right)^* \circ \mathcal{F}\left(\omega_y^{k+1}\right) - \mathcal{F}\left(\nabla_x^2\right)\gamma_1^k - \mathcal{F}\left(\nabla_y^2\right)\gamma_2^k}{2\alpha_1 \mathcal{F}(I) + \beta\mathcal{F}\left(\nabla_x^2\right)^* \circ \mathcal{F}\left(\nabla_x^2\right) + \beta\mathcal{F}\left(\nabla_y^2\right)^* \circ \mathcal{F}\left(\nabla_y^2\right)}\right\}, \tag{21}$$

where "$*$" denotes complex conjugacy, "$\circ$" denotes component-wise multiplication, $\nabla^{2^T} = (\nabla_x^{2^T}, \nabla_y^{2^T}), \gamma^k = (\gamma_1^k, \gamma_2^k)$, and $\mathcal{F}^{-1}$ is the inverse Fourier transform.

Finally, we update Lagrange multiplier γ:

$$\gamma^{k+1} = \gamma^k - \beta\left(\omega^{k+1} - \nabla^2 f^{k+1}\right). \tag{22}$$

Our method in this paper can be described as shown in Algorithm 1.

3. Numerical Experiments

In this section, we present some numerical examples of image restoration to illustrate the effectiveness of our proposed approach. In our experiments, we compare the proposed algorithm with the other three state-of-the-art methods, namely, FCP [44], high-order TV [45], and SALSA [43], under three different blurring operators. All experiments are performed under Windows 10 and MATLAB 2012a running on a desktop with an Intel® Core i5 Duo central processing unit at 2.50 GHz and 4 GB memory. The signal-to-noise ratio (SNR), the structural similarity index measurement (SSIM) [67], and the blurred signal to noise ratio (BSNR) are employed to measure the quality of the restored images by different algorithms. They are defined as follows:

$$\begin{aligned} SNR &= 20 * \log_{10}\frac{\left\|f^0 - \overline{f}\right\|_2}{\left\|f^0 - f\right\|_2}, \\ BSNR &= 20 * \log_{10}\frac{\|g\|_2}{\|\eta\|_2}, \\ SSIM &= \frac{\left(2\mu_{f^0}\mu_f + c_1\right)\left(2\sigma_{f^0 f} + c_2\right)}{\left(\mu_{f^0}^2 + \mu_f^2 + c_1\right)\left(\sigma_{f^0}^2 + \sigma_f^2 + c_2\right)}, \end{aligned} \tag{23}$$

where f^0, f, and η are the original image, the restored image, and the noise vector added in the test, respectively. $\overline{f}$ is the mean intensity value of f^0, μ_{f^0} and μ_f are the mean value of f^0 and f, respectively. $\sigma_{f^0}^2$ and σ_f^2 are the variance of f^0 and f, respectively. And $\sigma_{f^0 f}$ is covariance of f^0 and f. c_1 and c_2 are constants. The SSIM is an index used to measure the similarity between restored image and ideal image. The closer the SSIM value to 1, the better the restored image.

Three classical grayscale images, named, "Lena" (256× 256), "Man" (512× 512), and "Cameraman" (256× 256), are used as the test images and shown in Figure 1. To make it easier to compare different methods, we set $\|f^{k+1} - f^k\|_2 / \|f^k\|_2 \leq 1 \times 10^{-5}$ as the stopping criterion in all experiments.

(a) Lena (b) Man (c) Cameraman

Figure 1: Test images.

3.1. Parameters Settings. In this subsection, we discuss the selection of the three regularization parameters α_1, α_2, and α_3 in our method. In order to explain how to choose parameters in our algorithm, we recover the "Lena" image, which is blurred by Gaussian blur with size "9× 9" and added the Gaussian white noise with BSNR=35. The influence of different α_1, α_2, and α_3 on the restoration image is explained in Figure 2. As shown in Figure 2, if α_1 is too small, the restored image will be overly smoothed with smeared image details. In contrast, the restored image will be dominated by noise component with larger α_1 values. We can see from Figures 2(e) and 2(f) that when the parameter α_2 changes within a certain range, there is little effect on image restoration. The parameter α_3 has the same effect as the one of α_1 has. The restored image will be overly smoothed with small α_3 values and dominated by noise component with larger α_3 values. The parameters α_1, α_2, and α_3 in our method are manually adjusted to the optimal value. Therefore, the parameters used in the tests will be illustrated in the following experiments.

3.2. Gaussian Blur. In this example, we consider the Gaussian blur. The "Man" image shown in Figure 3(b) is degraded by Gaussian blur. The function has two parameters: bandwidth s and standard deviation σ. In the test, we choose $s = \sigma = 7$. We added Gaussian noise with BSNR = 35 to the test image. The parameters $\lambda = 0.025$ and $\mu = 0.35$ are selected in SALSA. The parameters $\alpha_1 = 0.02$, $\alpha_2 = 0.001$, and $\alpha_3 = 0.02$ are selected in our method. The parameters $\alpha_1 = 0.015$, $\alpha_2 = 0.2$, and $\alpha_3 = 0.05$ are used in FCP method. For the high-order TV method, the parameters $\alpha_1 = 0.8$ and $\alpha_2 = 0.005$ are selected. The restored images obtained by SALSA [43], FCP [44], high-order TV [45], and our method are shown in Figures 3(c)–3(f). The changing curve of SNR of the reconstructed image during the experiment is shown in Figure 4. It can be seen from the changing graph that our method can get higher SNR than the other three methods. In Table 1, we list the restoration results of the four different methods in SNRs and SSIMs. From Figures 3(c)–3(f), we can see that the SALSA method can make restoration image smooth, the FCP method causes staircase effect, and our method can induce sparse structure of the image compared with the high-order TV method. The visual quality of the restored image by our method is better than the other three methods. More precisely, the same regions of image are zoomed and processed in the same way; they are presented in Figure 5. It is not difficult to see that our method has some advantages over the other three methods in eliminating the staircase effect.

3.3. Average Blur. In this example, we choose "Cameraman" image with size 256 × 256 as an object of study. The image is degraded by average kernel with window size 11 and contaminated by the Gaussian noise with BSNR = 40, which is shown in Figure 6(b). In this example, we choose the parameters $\lambda = 0.045$ and $\mu = 0.35$ for SALSA method. The parameters $\alpha_1 = 0.02$,$\alpha_2 = 0.01$, and $\alpha_3 = 0.02$ are used in our method. The parameters $\alpha_1 = 0.008$, $\alpha_2 = 0.3$, and $\alpha_3 = 0.05$ are selected in FCP method. For high-order TV, the parameters $\alpha_1 = 1.5$ and $\alpha_2 = 0.005$ are used. Figures 6(c)–6(f) represent the restored images by SALSA, FCP, high-order TV, and our method, respectively. The change of SNR of the reconstructed image during the experiment is shown in Figure 7. The experimental results on SNR and SSIM are shown in Table 1. We see that both the SNR and SSIM values of the restored image by our method are higher than those provided by the SALSA [43], FCP [44], and high-order TV [45] method. The quality of restored images by our method is better than the other three methods.

Our method has some advantages in detail processing. In Figure 6, we have enlarged some details of image. The recovery results are presented in Figures 8(b)–8(e). Obviously, our method can well overcome the staircase effect and retain more image details.

3.4. Disk Blur. For this experiment, we consider the well-known "Lena" as the test image. The image is corrupted by the Gaussian noise with BSNR = 35. The PSF for the linear disk blur represented a line segment of radius r. In this experiment, we select $r = 7$. The original image and the observed image are shown in Figures 9(a) and 9(b). The parameters $\alpha_1 = 0.035$, $\alpha_2 = 0.03$, and $\alpha_3 = 0.02$ are selected

Figure 2: The restoration results for different parameters. (a) Original image. (b) Observed image: the "Lena" image is blurred by Gaussian blur with size "9× 9" and added the Gaussian noise with BSNR=35. (c) The restoration result with $\alpha_1 = 2e-1$, $\alpha_2 = 3e-3$, and $\alpha_3 = 2e-3$ (SNR = 22.04). (d) The restoration result with $\alpha_1 = 2e-5$, $\alpha_2 = 3e-3$, and $\alpha_3 = 2e-3$ (SNR = 19.97). (e) The restoration result with $\alpha_1 = 2e-3$, $\alpha_2 = 3e-1$, and $\alpha_3 = 2e-3$ (SNR = 22.51). (f) The restoration result with $\alpha_1 = 2e-3$, $\alpha_2 = 3e-5$, and $\alpha_3 = 2e-3$ (SNR = 22.49). (g) The restoration result with $\alpha_1 = 2e-3$, $\alpha_2 = 3e-3$, and $\alpha_3 = 2e-1$ (SNR = 19.73). (h) The restoration result with $\alpha_1 = 2e-3$, $\alpha_2 = 3e-3$, and $\alpha_3 = 2e-5$ (SNR = 16.88). (i) The restoration result with $\alpha_1 = 2e-3$, $\alpha_2 = 3e-3$, and $\alpha_3 = 2e-3$ (SNR = 22.92).

Table 1: The values of SNR and SSIM for different experiments.

Blur	Image	SALSA [43]		FCP [44]		High-order TV [45]		Our	
		SNR	SSIM	SNR	SSIM	SNR	SSIM	SNR	SSIM
Gaussian	man	23.91	0.6431	24.22	0.6522	24.60	0.6663	25.13	0.7034
	cameraman	25.92	0.6537	26.31	0.6872	26.83	0.7324	27.69	0.7868
	Lena	23.19	0.6580	23.37	0.6724	23.84	0.7047	24.56	0.7503
Average	man	22.31	0.6087	22.61	0.6290	23.18	0.6826	23.77	0.7392
	cameraman	20.38	0.5760	20.64	0.5977	20.89	0.6300	21.47	0.6915
	Lena	22.15	0.5986	22.39	0.6150	22.82	0.6559	23.58	0.6868
Disk	man	21.96	0.5267	22.26	0.5429	22.67	0.5671	23.10	0.5872
	cameraman	20.10	0.5613	20.37	0.5758	20.85	0.6023	21.21	0.6173
	Lena	20.24	0.5873	20.50	0.5921	20.78	0.6325	21.27	0.6443

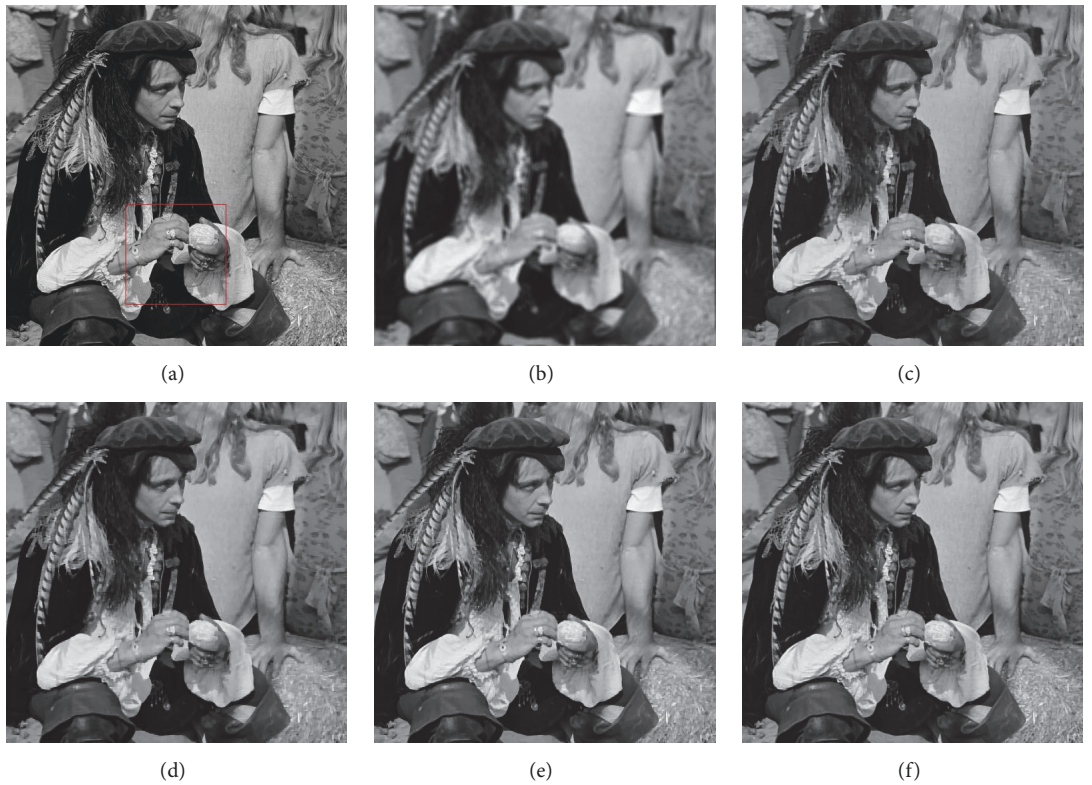

Figure 3: Image restoration in Gaussian blur. (a) Original image; (b) blurred and noisy image; (c) image deblurred by SALSA [43]; (d) image deblurred by FCP [44]; (e) image deblurred by high-order TV [45]; (f) image deblurred by our method.

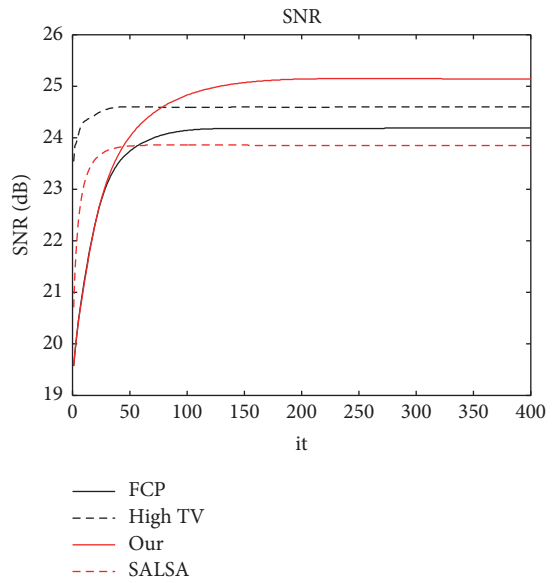

Figure 4: SNR versus iterations with four different methods.

in our method. In parameters, we set $\lambda = 0.035$ and $\mu = 0.5$ for SALSA method. The parameters $\alpha_1 = 0.008$, $\alpha_2 = 0.05$, and $\alpha_3 = 0.015$ are used in FCP method. For the high-order TV method, the parameters $\alpha_1 = 1.2$ and $\alpha_2 = 0.005$ are selected. The restored images by the SALSA, FCP, high-order TV, and our method are shown in Figures 9(c)–9(f). In Figure 10, we plot the changes of SNR value versus iteration number for the four methods. Figure 11 shows the enlarged results of a part of Figure 9. The values of SNR and SSIM are listed in Table 1. We can see that our method can reduce the staircase effect effectively while preserving the edges.

We can see from the above three experiments that the images restored by our method have better qualities with less staircase effect and more detail textures than the other three

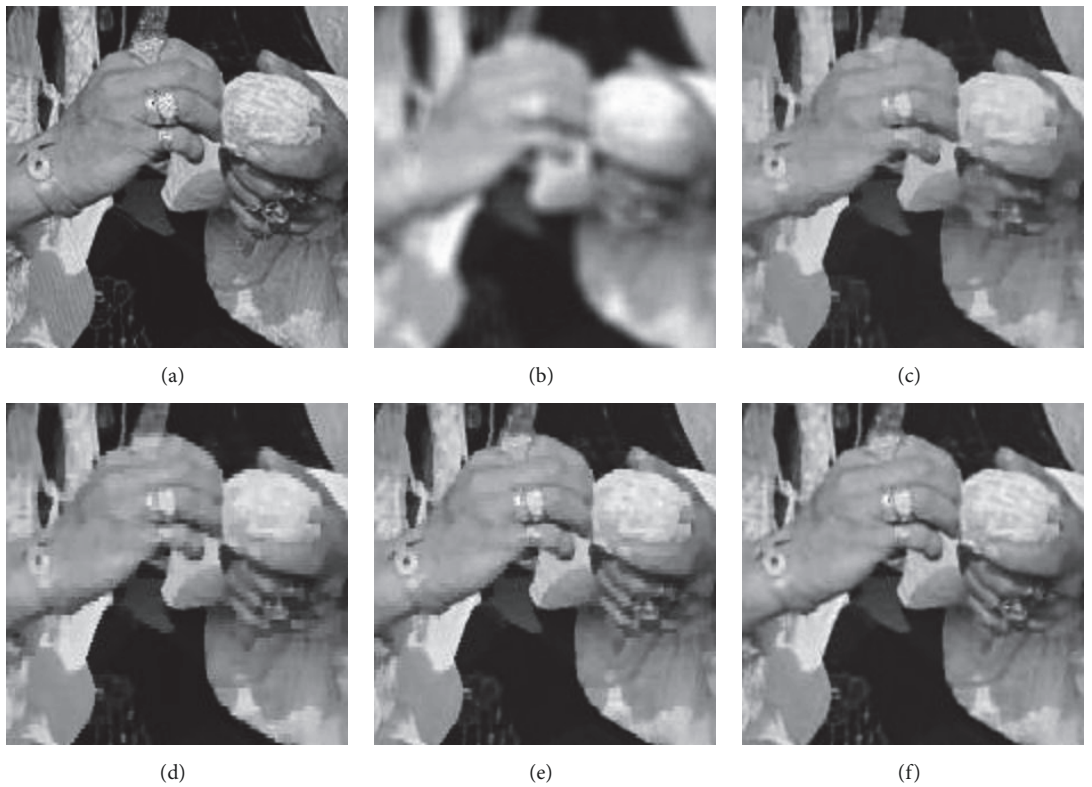

(a) (b) (c)

(d) (e) (f)

Figure 5: The zoomed regions of the results of Figure 3. (a) Original region; (b) blurred and noisy image; (c) restoration region of SALSA [43]; (d) restoration region of FCP [44]; (e) restoration region of high-order TV [45]; (f) restoration region of our method.

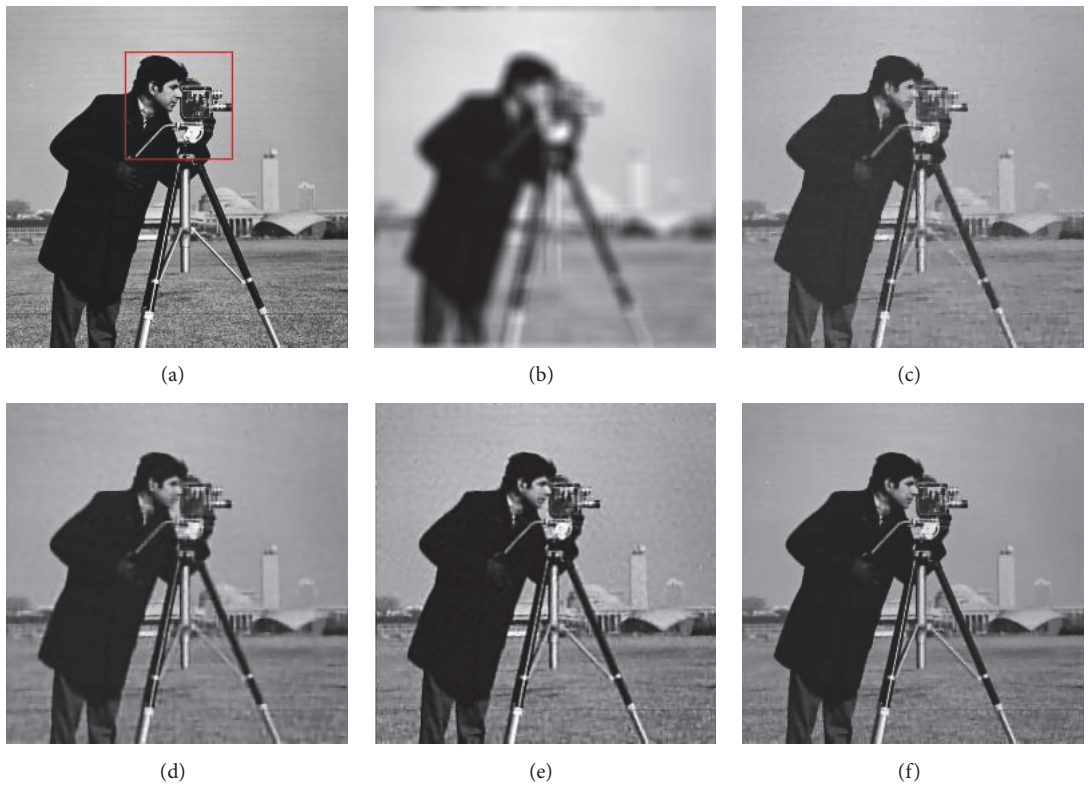

(a) (b) (c)

(d) (e) (f)

Figure 6: Image restoration in average blur. (a) Original image; (b) blurred and noisy image; (c) image deblurred by SALSA [43]; (d) image deblurred by FCP [44]; (e) image deblurred by high-order TV [45]; (f) image deblurred by our method.

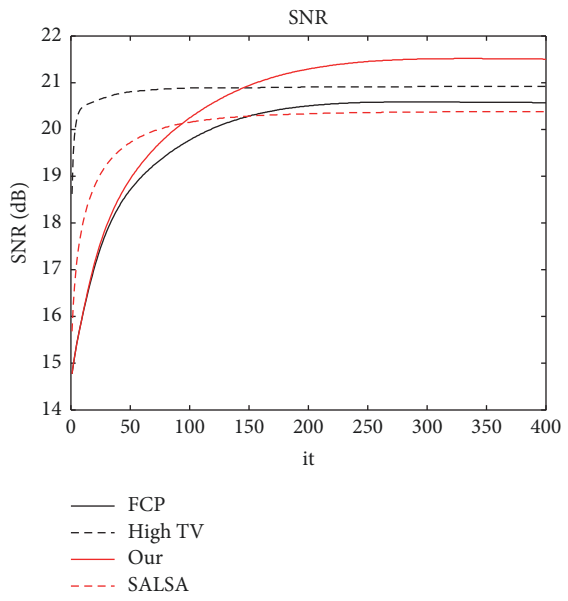

Figure 7: SNR versus iterations with four different methods.

Figure 8: The zoomed regions of the results of Figure 6. (a) Original region; (b) blurred and noisy image; (c) restoration region of SALSA [43]; (d) restoration region of FCP [44]; (e) restoration region of high-order TV [45]; (f) restoration region of our method.

methods. In order to further verify the effectiveness of our method, for the same experiment, we tested all the images which are listed in Figure 1, and the experimental results are shown in Table 1. We can find from the experimental results that the SNR and SSIM values obtained by our method are higher than the other three methods.

4. Conclusion

In this paper, by combining high-order total variation regularization and l_1 regularization, we propose a new variational model. Numerical experiments show that our method can overcome the staircase effects while

Figure 9: Image restoration in disk blur. (a) Original image; (b) blurred and noisy image; (c) image deblurred by SALSA [43]; (d) image deblurred by FCP [44]; (e) image deblurred by high-order TV [45]; (f) image deblurred by our method.

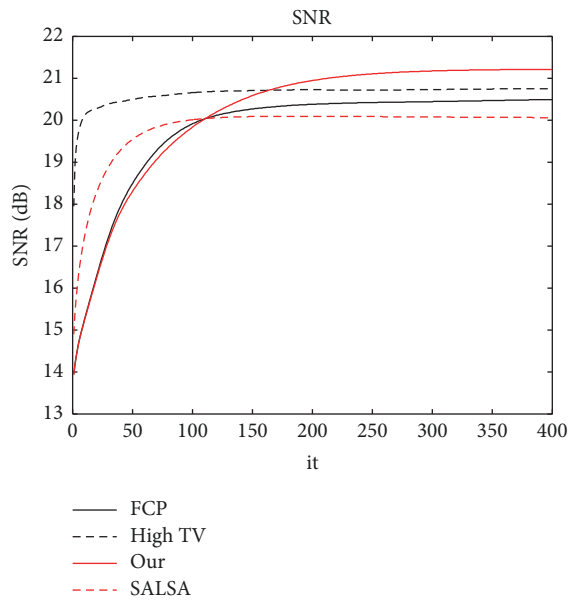

Figure 10: SNR versus iterations with four different methods.

preserving edges of the restored image. We also show that our proposed method can obtain better results than the three state-of-the-art methods with higher SSIM and SNR values.

Data Availability

The test images in the article can be freely downloaded from this site "http://sipi.usc.edu/database/".

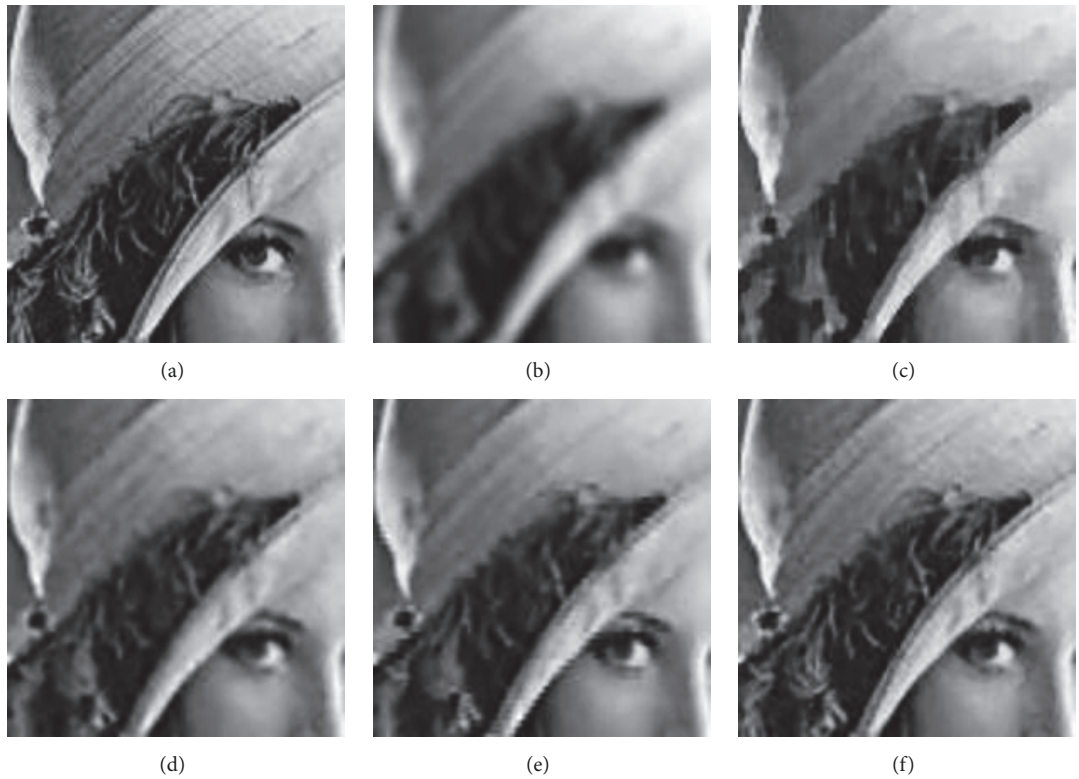

Figure 11: The zoomed regions of the results of Figure 9. (a) Original region; (b) blurred and noisy image; (c) restoration region of SALSA [43]; (d) restoration region of FCP [44]; (e) restoration region of high-order TV [45]; (f) restoration region of our method.

Conflicts of Interest

The authors declare that they have no conflicts of interest.

Acknowledgments

This work was supported by the Training Program of the Major Research Plan of National Science Foundation of China under Grant 91746104, by National Science Foundation of China under Grant 61101208 and Grant 11326186, by Qingdao Postdoctoral Science Foundation, China (2016114), by a project of Shandong Province Higher Educational Science and Technology Program, China (J17KA166), and by Joint Innovative Center for Safe and Effective Mining Technology and Equipment of Coal Resources, Shandong Province of China, and SDUST Research Fund (2014TDJH102).

References

[1] H. Tanaka, T. Hayashi, and T. Nishi, "Application of digital image analysis to pattern formation in polymer systems," *Journal of Applied Physics*, vol. 59, no. 11, pp. 3627–3643, 1986.

[2] T. Li, X. Li, J. Wang et al., "Nonlinear sinogram smoothing for low-dose X-ray CT," *IEEE Transactions on Nuclear Science*, vol. 51, no. 5, pp. 2505–2513, 2004.

[3] M. Chen and G. Li, "Forming mechanism and correction of CT image artifacts caused by the errors of three system parameters," *Journal of Applied Mathematics*, vol. 2013, Article ID 545147, 7 pages, 2013.

[4] Y. Chen, Y. Guo, Y. Wang, D. Wang, C. Peng, and G. He, "Denoising of Hyperspectral Images Using Nonconvex Low Rank Matrix Approximation," *IEEE Transactions on Geoscience and Remote Sensing*, vol. 55, no. 9, pp. 5366–5380, 2017.

[5] H. Chen, C. Wang, Y. Song, and Z. Li, "Split Bregmanized anisotropic total variation model for image deblurring," *Journal of Visual Communication and Image Representation*, vol. 31, pp. 282–293, 2015.

[6] A. N. Tikhonov and V. Y. Arsenin, *Solution of Ill-Posed Problems*, Winston, 1977.

[7] L. I. Rudin, S. Osher, and E. Fatemi, "Nonlinear total variation based noise removal algorithms," *Physica D: Nonlinear Phenomena*, vol. 60, no. 1–4, pp. 259–268, 1992.

[8] C. R. Vogel and M. E. Oman, "Iterative methods for total variation denoising," *SIAM Journal on Scientific Computing*, vol. 17, no. 1, pp. 227–238, 2012.

[9] Q. Li, L. Shen, Y. Xu, and N. Zhang, "Multi-step fixed-point proximity algorithms for solving a class of optimization problems arising from image processing," *Advances in Computational Mathematics*, vol. 41, no. 2, pp. 387–422, 2015.

[10] J. Tang, G. He, L. Dong, L. Fang, and J. Zhou, "A smoothing Newton method for the second-order cone complementarity problem," *Applications of Mathematics*, vol. 58, no. 2, pp. 223–247, 2013.

[11] L. Sun, G. He, Y. Wang, and C. Zhou, "An accurate active set Newton algorithm for large scale bound constrained optimization," *Applications of Mathematics*, vol. 56, no. 3, pp. 297–314, 2011.

[12] J. Yu, M. Li, Y. Wang, and G. He, "A decomposition method for large-scale box constrained optimization," *Applied Mathematics and Computation*, vol. 231, no. 12, pp. 9–15, 2014.

[13] C. Han, F. Zheng, T. Guo, and G. He, "Parallel algorithms for large-scale linearly constrained minimization problem," *Acta Mathematicae Applicatae Sinica*, vol. 30, no. 3, pp. 707–720, 2014.

[14] L. Sun, L. Fang, and G. He, "An active set strategy based on the multiplier function or the gradient," *Applications of Mathematics*, vol. 55, no. 4, pp. 291–304, 2010.

[15] T. F. Chan, G. H. Golub, and P. Mulet, "A nonlinear primal-dual method for total variation-based image restoration," *SIAM Journal on Scientific Computing*, vol. 20, no. 6, pp. 1964–1977, 1999.

[16] A. Chambolle, "An algorithm for total variation minimization and applications," *Journal of Mathematical Imaging and Vision*, vol. 20, no. 1-2, pp. 89–97, 2004.

[17] G. Yu, L. Qi, and Y. Dai, "On nonmonotone Chambolle gradient projection algorithms for total variation image restoration," *Journal of Mathematical Imaging and Vision*, vol. 35, no. 2, pp. 143–154, 2009.

[18] M. Li, C. Han, R. Wang, and T. Guo, "Shrinking gradient descent algorithms for total variation regularized image denoising," *Computational Optimization and Applications*, vol. 68, no. 3, pp. 643–660, 2017.

[19] J. M. Bioucas-Dias and M. A. T. Figueiredo, "A new TwIST: two-step iterative shrinkage/thresholding algorithms for image restoration," *IEEE Transactions on Image Processing*, vol. 16, no. 12, pp. 2992–3004, 2007.

[20] M. Elad, B. Matalon, and M. Zibulevsky, "Coordinate and subspace optimization methods for linear least squares with non-quadratic regularization," *Applied and Computational Harmonic Analysis* , vol. 23, no. 3, pp. 346–367, 2007.

[21] B. Hao and J. Zhu, "Fast L1 regularized iterative forward backward splitting with adaptive parameter selection for image restoration," *Journal of Visual Communication and Image Representation*, vol. 44, pp. 139–147, 2017.

[22] I. Daubechies, M. Defrise, and C. de Mol, "An iterative thresholding algorithm for linear inverse problems with a sparsity constraint," *Communications on Pure and Applied Mathematics*, vol. 57, no. 11, pp. 1413–1457, 2004.

[23] J. G. Zhu and B. B. Hao, "A new noninterior continuation method for solving a system of equalities and inequalities," *Journal of Applied Mathematics*, vol. 2014, Article ID 592540, 6 pages, 2014.

[24] J. L. Starck, M. K. Nguyen, and F. Murtagh, "Wavelets and curvelets for image deconvolution: a combined approach," *Signal Processing*, vol. 83, no. 10, pp. 2279–2283, 2003.

[25] Y. Wang, J. Yang, W. Yin, and Y. Zhang, "A new alternating minimization algorithm for total variation image reconstruction," *SIAM Journal on Imaging Sciences*, vol. 1, no. 3, pp. 248–272, 2008.

[26] X. Zhang, M. Burger, and X. Bresson, "Bregmanized nonlocal regularization for deconvolution and sparse reconstruction," *SIAM Journal on Imaging Sciences*, vol. 3, no. 3, pp. 253–276, 2010.

[27] Z. Tian, M. Tian, Z. Liu, and T. Xu, "The Jacobi and Gauss-Seidel-type iteration methods for the matrix equation AXB=C," *Applied Mathematics and Computation*, vol. 292, pp. 63–75, 2017.

[28] S. Setzer, G. Steidl, and T. Teuber, "Deblurring Poissonian images by split Bregman techniques," *Journal of Visual Communication and Image Representation*, vol. 21, no. 3, pp. 193–199, 2010.

[29] Z. Feng, L. Fang, and G. He, "An O(nL) iteration primal-dual path-following method, based on wide neighbourhood and large update, for second-order cone programming," *Optimization*, vol. 63, no. 5, pp. 679–691, 2014.

[30] J. Yang, Y. Zhang, and W. Yin, "A fast alternating direction method for TVL1-L2 signal reconstruction from partial Fourier data," *IEEE Journal of Selected Topics in Signal Processing*, vol. 4, no. 2, pp. 288–297, 2010.

[31] M. Tao and J. Yang, "Alternating direction algorithms for total variation deconvolution in image reconstruction," Technical report tr0918, Department of Mathematics, Nanjing University, 2009, http://www.optimization-online.org/DB_FILE/2009/11/2463.pdf.

[32] C. Q. Miao, "Computing eigenpairs in augmented Krylov subspace produced by Jacobi–Davidson correction equation," *Journal of Computational and Applied Mathematics*, vol. 343, pp. 363–372, 2018.

[33] D. Gabay and B. Mercier, "A dual algorithm for the solution of nonlinear variational problems via finite element approximation," *Computers & Mathematics with Applications*, vol. 2, no. 1, pp. 17–40, 1976.

[34] R. Y. Zhang, F. F. Xu, and J. C. Huang, "Reconstructing local volatility using total variation," *Acta Mathematica Sinica*, vol. 33, no. 2, pp. 263–277, 2017.

[35] Z. Bai, X. Dong, and C. Yin, "Existence results for impulsive nonlinear fractional differential equation with mixed boundary conditions," *Boundary Value Problems*, vol. 2016, p. 63, 2016.

[36] W. X. Ma and Y. Zhou, "Lump solutions to nonlinear partial differential equations via Hirota bilinear forms," *Journal of Differential Equations*, vol. 264, no. 4, pp. 2633–2659, 2018.

[37] Z. Wang, "A Numerical Method for Delayed Fractional-Order Differential Equations," *Journal of Applied Mathematics*, vol. 2013, Article ID 256071, 7 pages, 2013.

[38] Z. Wang, X. Huang, and J. P. Zhou, "A numerical method for delayed fractional-order differential equations: based on G-L definition," *Applied Mathematics & Information Sciences*, vol. 7, no. 2, pp. 525–529, 2013.

[39] C. Jiang, F. Zhang, and T. Li, "Synchronization and anti-synchronization of N-coupled fractional-order complex systems with ring connection," *Mathematical Methods in the Applied Sciences*, vol. 41, no. 7, pp. 2625–2638, 2018.

[40] M. R. Hajiaboli, "An anisotropic fourth-order diffusion filter for image noise removal," *International Journal of Computer Vision*, vol. 92, no. 2, pp. 177–191, 2011.

[41] Y. Zhang, M. Zhao et al., "Novel model for cascading failure based on degree strength and its application in directed genelogic networks," *Computational and Mathematical Methods in Medicine*, vol. 2018, Article ID 8950794, 9 pages, 2018.

[42] G. Lyu, H. Yin, X. Yu, and S. Luo, "A local characteristic image restoration based on convolutional neural network," *IEICE Transaction on Information and Systems*, vol. 99, no. 8, pp. 2190–2193, 2016.

[43] M. V. Afonso, J. M. Bioucas-Dias, and M. A. T. Figueiredo, "Fast image recovery using variable splitting and constrained optimization," *IEEE Transactions on Image Processing*, vol. 19, no. 9, pp. 2345–2356, 2010.

[44] S. Wang, T.-Z. Huang, J. Liu, and X.-G. Lv, "An alternating iterative algorithm for image deblurring and denoising problems," *Communications in Nonlinear Science and Numerical Simulation*, vol. 19, no. 3, pp. 617–626, 2014.

[45] X. G. Lv, Y. Z. Song, S. X. Wang, and J. Le, "Image restoration with a high-order total variation minimization method," *Applied Mathematical Modelling*, vol. 37, no. 16-17, pp. 8210–8224, 2013.

[46] Y. M. Huang, M. K. Ng, and Y. W. Wen, "A fast total variation minimization method for image restoration," *Multiscale Modeling & Simulation*, vol. 7, no. 2, pp. 774–795, 2008.

[47] A. Chambolle and P.-L. Lions, "Image recovery via total variation minimization and related problems," *Numerische Mathematik*, vol. 76, no. 2, pp. 167–188, 1997.

[48] T. Chan, A. Marquina, and P. Mulet, "High-order total variation-based image restoration," *Society for Industrial and Applied Mathematics*, vol. 22, no. 2, pp. 503–516, 2000.

[49] K. Papafitsoros and C. B. Schönlieb, "A combined first and second order variational approach for image reconstruction," *Journal of Mathematical Imaging and Vision*, vol. 48, no. 2, pp. 308–338, 2014.

[50] K. Bredies, K. Kunisch, and T. Pock, "Total generalized variation," *SIAM Journal on Imaging Sciences*, vol. 3, no. 3, pp. 492–526, 2010.

[51] S. Lefkimmiatis, A. Bourquard, and M. Unser, "Hessian-based norm regularization for image restoration with biomedical applications," *IEEE Transactions on Image Processing*, vol. 21, no. 3, pp. 983–995, 2012.

[52] G. Steidl, "A note on the dual treatment of higher-order regularization functionals," *Computing*, vol. 76, no. 1-2, pp. 135–148, 2006.

[53] M. Lysaker, A. Lundervold, and X. C. Tai, "Noise removal using fourth-order partial differential equation with applications to medical magnetic resonance images in space and time," *IEEE Transactions on Image Processing*, vol. 12, no. 12, pp. 1579–1589, 2003.

[54] C. Wu and X. C. Tai, "Augmented Lagrangian method, dual methods, and split Bregman iteration for ROF, vectorial TV, and high order models," *SIAM Journal on Imaging Sciences*, vol. 3, no. 3, pp. 300–339, 2010.

[55] A. Beck and M. Teboulle, "A fast iterative shrinkage-thresholding algorithm for linear inverse problems," *SIAM Journal on Imaging Sciences*, vol. 2, no. 1, pp. 183–202, 2009.

[56] M. Li, X. Kao, and H. Che, "Relaxed inertial accelerated algorithms for solving split equality feasibility problem," *Journal of Nonlinear Sciences and Applications*, vol. 10, no. 8, pp. 4109–4121, 2017.

[57] C. H. Liu, Y. L. Shang, and P. Han, "A new infeasible-interior-point algorithm for linear programming over symmetric cones," *Acta Mathematicae Applicatae Sinica*, vol. 33, no. 3, pp. 771–788, 2017.

[58] B. Deng, T. Chen, and B. Xin, "Parallel and cyclic algorithms for quasi-nonexpansives in hilbert space," *Abstract and Applied Analysis*, vol. 2012, Article ID 218341, 27 pages, 2012.

[59] F. Zheng, C. Han, and Y. Wang, "Parallel SSLE algorithm for large scale constrained optimization," *Applied Mathematics Computation*, vol. 217, no. 12, pp. 5377–5384, 2011.

[60] C. Han, T. Feng, G. He, and T. Guo, "Parallel variable distribution algorithm for constrained optimization with nonmonotone technique," *Journal of Applied Mathematics*, vol. 2013, Article ID 295147, 7 pages, 2013.

[61] L. Sun, G. He, Y. Wang, and L. Fang, "An active set quasi-Newton method with projected search for bound constrained minimization," *Computers Mathematics with Applications*, vol. 58, no. 1, pp. 161–170, 2009.

[62] Z. L. Tian, M. Tian, C. Gu, and X. Hao, "An accelerated jacobi-gradient based iterative algorithm for solving sylvester matrix equations," *Filomat*, vol. 31, no. 8, pp. 2381–2390, 2017.

[63] A. Beck and M. Teboulle, "Fast gradient-based algorithms for constrained total variation image denoising and deblurring problems," *IEEE Transactions on Image Processing*, vol. 18, no. 11, pp. 2419–2434, 2009.

[64] J. Yang, W. Yin, Y. Zhang, and Y. Wang, "A fast algorithm for edge-preserving variational multichannel image restoration," *SIAM Journal on Imaging Sciences*, vol. 2, no. 2, pp. 569–592, 2009.

[65] M. K. Ng, R. H. Chan, and W.-C. Tang, "A fast algorithm for deblurring models with Neumann boundary conditions," *SIAM Journal on Scientific Computing*, vol. 21, no. 3, pp. 851–866, 1999.

[66] R. C. Gonzalez and R. E. Woods, *Digital Image Processing*, Addison-Wesley, Reading, MA, USA, 3rd edition, 2007.

[67] Z. Wang, A. C. Bovik, H. R. Sheikh, and E. P. Simoncelli, "Image quality assessment: from error visibility to structural similarity," *IEEE Transactions on Image Processing*, vol. 13, no. 4, pp. 600–612, 2004.